A&A 454, 1–9 (2006)
DOI: 10.1051/0004-6361:20054572

Astronomy & Astrophysics

Cosmic ray transport in anisotropic magnetohydrodynamic turbulence

IV. Steep wave spectra⋆

A. Shalchi and R. Schlickeiser

Institut für Theoretische Physik, Lehrstuhl IV: Weltraum- und Astrophysik, Ruhr-Universität Bochum, 44780 Bochum, Germany

Received 23 November 2005 / Accepted 1 March 2006

ABSTRACT

By calculating the heating rate of the interstellar medium a recent paper argued that the wave spectrum of the turbulent magnetic fields could be steeper than $k^{-5/3}$. Although this behaviour disagrees with the Kolmogorv theory of turbulence, a steep inertial range of the wave spectrum in the interstellar medium cannot be excluded by obervations. In this paper, we therefore explore the influence of steep spectra onto the momentum diffusion coefficient and onto the parallel mean free path of cosmic rays. The calculations presented in this paper use the quasilinear theory, which can be seen as the standard tool computing cosmic-ray diffusion coefficients. As in earlier papers we consider an anisotropic plasma-wave turbulence model. It is demonstrated that momentum and parallel spatial diffusion are quite different, if the inertial range spectral index is larger than the Kolmogorov value.

Key words. magnetohydrodynamics (MHD) – plasmas – turbulence – ISM: cosmic rays – ISM: magnetic fields

1. Introduction

In the first paper of this series (Lerche & Schlickeiser 2001), we started to evaluate relevant cosmic ray transport parameters in the presence of anisotropic fast magnetosonic plasma-wave turbulence. All technical details for calculating Fokker-Planck coefficients and their relation to the transport parameters of the cosmic-ray diffusion-convection equation, as the parallel mean free path and the momentum diffusion coefficient, were presented there. In the second (Teufel et al. 2003) and third papers (Shalchi & Schlickeiser 2004a) of the series, we repeated the calculations for shear Alfvén waves and a mixed turbulence model that consists of a magnetosonic and an Alfvénic contribution. In order to avoid unnecessary repititions, we use the same notation as in the three earlier papers and we frequently refer to equations in these papers. In all three papers we restricted our calculations to flat wave spectra ($s < 2$) and to small and medium rigidities ($R_{\rm L} k_{\rm min} \ll 1$) corresponding to cosmic-ray total energies

$$E \leq E_K = 6 \times 10^{14} Z B_{\mu G}^{-1} \left(k_{\rm min}^{-1} / 2 \times 10^{18}\ {\rm cm}^{-1} \right) \quad (1)$$

slightly below the knee in the cosmic-ray energy spectrum. Here we explore the case of steep wave spectra ($s > 2$) motivated by previous theoretical considerations as described in the next section.

2. The form of wave spectra in the interstellar medium concluded from heating-rate calculations

A key input into cosmic-ray transport theories is the correlation tensor (or power spectrum) of magnetic field fluctuations

$$P_{lm}(\boldsymbol{k}, t) = \left\langle \delta B_l(\boldsymbol{k}, t) \delta B_m^*(\boldsymbol{k}, 0) \right\rangle . \quad (2)$$

⋆ Appendices are only available in electronic form at http://www.edpsciences.org

Knowledge of this tensor allows calculation of diffusion coefficients like the momentum diffusion coefficient A or the parallel mean free path $\lambda_\parallel$ within a transport theory, such as the quasilinear theory (QLT, Jokipii 1966). The correlation tensor is determined by specifying the turbulence geometry, the wave spectrum, and the dynamical correlation function, which describes the time dependence of P_{lm}. While different models for the geometry and dynamical correlation function have been discussed in the past, the wave spectrum was assumed to be known. If transport of heliopheric cosmic rays is described, the wave spectrum can be obtained from observations (see e.g. Denskat & Neubauer 1982). In the case of the solar wind, a spectral index of $s = 5/3$ was observed, in agreement with the Kolmogorv (1941) turbulence theory. Only small deviations from $s = 5/3$ are possible, such as more Kraichnan-Iroshnikov (1965)-like behaviour ($s = 3/2$). Although the heliospheric wave spectrum cannot be too different from the observed $k^{-5/3}$-law, not much is known about the wave spectrum in the interstellar medium (ISM). Because of heliospheric observations and several theoretical discussions (like the Kolmogorov theory), a value $s = 5/3$ was the standard assumption in the ISM.

The power spectra of the magnetic fields in the ISM cannot be measured directly. Only the power spectrum of interstellar electron density fluctuations is accessible via radio scintillation and dispersion measure studies (Armstrong et al. 1995), and it indeed has a Kolmogorov form $P_n \propto k^{-5/3}$ over more than 10 decades of wavenumber values; therefore, the relation between magnetic field fluctuations and electron density fluctuations has to be investigated. For fast and slow magnetosonic waves in the low-beta diffuse ISM-phase, both classical MHD theory (Dogan et al. 2005) and kinetic plasma-wave theory (Schlickeiser & Lerche 2002) exhibit a direct correspondence $P_n^M(k)/n_{\rm e}^2 \simeq P_{zz}(k)/B_0^2$ between the parallel tensor components of the electron density and the magnetic field fluctuations.

This implies that the correlation tensor of the magnetic fluctuations varies as $P_{zz}(k) \propto k^{-5/3}$ for magnetosonic waves. Shear Alfvén waves are incompressible according to classical MHD theory, but become compressive in kinetic plasma-wave theory with the wavenumber-dependent relation $P_n^{\rm A}(k)/n_{\rm e}^2 \simeq (kV_{\rm A}/\Omega_p)^2(P_{yy}(k)/B_0^2)$, so that the implied magnetic field correlation tensor of shear Alfvén waves varies as $P_{yy}(k) \propto k^{-11/3}$.

Another important constraint on interstellar magnetic power spectra is provided by considering the heating of the diffuse interstellar medium by (mainly viscous) plasma-wave damping (Lazar et al. 2003; Spanier & Schlickeiser 2005; Lerche et al. 2005). In order not to exceed the known cooling rate of the diffuse ISM, it has been demonstrated by these papers that a flat power spectrum of magnetosonic waves (with isotropic distribution of wave vectors with respect to $\boldsymbol{B}_0$) cannot exist over more than 10 decades of wavenumber values. Either the flat ($\propto k^{-5/3}$) magnetosonic power spectrum cuts off at a wavenumber that is five orders of magnitude smaller than the standard high-wavenumber cutoff attributed to gyroresonant damping or, if it extends over more than 10 decades in wavenumer values, it has to be steeper than $\propto k^{-2.53}$ (see Spanier & Schlickeiser 2005, for details). The third possibility of having anisotropic wave-vector distributions and wavenumber-dependent cutoffs, as considered by Lerche et al. (2005), will be discussed in a further paper in this series. The scenario of interstellar wave turbulence adopted throughout this paper, which is consistent with all constraints and observations, is that the observed electron density fluctuations are mainly due to shear Alfvén waves and that magnetosonic waves provide a negligible contribution. As argued, the power spectra of all waves have to be rather steep ($s > 2$). It is the purpose of this paper to explore the consequences of parallel spatial diffusion and momentum diffusion of cosmic rays for such steep wave spectra.

It should be noted, however, that Yan & Lazarian (2004) have already discussed cosmic ray scattering and streaming in compressible magnetohydrodynamic turbulence. In this paper the authors used assumptions for the wave turbulence, which have been chosen to match numerical simulations of ISM turbulence. These assumptions do not agree with the turbulence parameters used in the current paper. Here we simply consider steep wave spectra as proposed by Lazar et al. (2003) and Spanier & Schlickeiser (2005), but the reader should keep in mind that these spectra do not agree with the values assumed in Yan & Lazarian (2004).

According to Lazar et al. (2003) and Spanier & Schlickeiser (2005), the spectral index for shear Alfvén waves is $s_{\rm A} \approx 2+5/3$ and $s_{\rm F} \approx 2.53$ for fast mode waves, if the turbulence is isotropic or slightly parallel oriented. In Sect. 3 we investigate the influence of this new behaviour on the momentum diffusion coefficient by applying quasilinear theory. For our calculations we use the same form of the wave spectrum as in the papers before:

$$I(\boldsymbol{k}) = \begin{cases} I_0 \left[k_\parallel^2 + \Lambda k_\perp^2\right]^{-(2+s)/2} & \text{for } \mid \boldsymbol{k} \mid \geq k_{\rm min} \\ 0 & \text{for } \mid \boldsymbol{k} \mid < k_{\rm min}, \end{cases}$$

but now we assume $2 < s < 4$. The parallel mean free path is calculated in Sect. 4 and the validity of quasilinear theory that is applied throughout the whole paper is discussed in Sect. 5.

3. Momentum diffusion coefficients for a steep wave spectrum

According to Schlickeiser (2002, Eqs. (12.3.24)–(12.3.30)), the momentum diffusion coefficient A can be calculated by using

$$A = \frac{1}{2}\int_{-1}^{+1} {\rm d}\mu \left[D_{pp} - \frac{D_{\mu p}^2}{D_{\mu\mu}}\right] \tag{3}$$

with the three Fokker-Planck coefficients D_{pp}, $D_{\mu p}$, and $D_{\mu\mu}$. For shear Alfvén waves and for fast mode waves and by assuming smallness for the parameter $\epsilon = v_{\rm A}/v \ll 1$, we have $D_{\mu\mu} \sim o(\epsilon^0)$, $D_{\mu p}^2 \sim o(\epsilon^4)$, $D_{pp} \approx \epsilon^2 p^2 D_{\mu\mu} \sim o(\epsilon^2)$, and therefore

$$A \approx \frac{\epsilon^2 p^2}{2}\int_{-1}^{+1} {\rm d}\mu\, D_{\mu\mu}. \tag{4}$$

Within this approximation, the knowledge of $D_{\mu\mu}$ allows determination of the parallel mean free path (see Sect. 4) and the momentum diffusion coefficient. All pitch-angle Fokker-Planck coefficients calculated in the current paper are symmetric in the pitch-angle cosine μ. Therefore we can define μ as a positive parameter and can use

$$A \approx \epsilon^2 p^2 \int_0^1 {\rm d}\mu\, D_{\mu\mu}. \tag{5}$$

By assuming a mixed turbulence model, all Fokker-Planck coefficients can be written as a superposition of an Alfvénic contribution $D_{ij}^{\rm A}$ and a fast magnetosonic contribution $D_{ij}^{\rm F}$:

$$D_{ij}^{\rm MIX} = D_{ij}^{\rm A} + D_{ij}^{\rm F}. \tag{6}$$

The Alfvénic Fokker-Planck coefficient of pitch-angle diffusion $D_{\mu\mu}^{\rm A}$ has been calculated in Teufel et al. (2003). There, a Kolmogorv-like wave spectrum was assumed but the results can also be applied to steep spectra. The fast mode coefficient $D_{\mu\mu}^{\rm F}$ consists of a transit-time damping contribution and a gyroresonance contribution. The total fast mode pitch-angle Fokker-Planck coefficient has the form

$$D_{\mu\mu}^{\rm F} = D_{\mu\mu}^{\rm T} + D_{\mu\mu}^{\rm G}, \tag{7}$$

so with Eq. (6) we obtain

$$A^{\rm F} = A^{\rm T} + A^{\rm G}. \tag{8}$$

The gyroresonance contribution $A^{\rm G}$ has already been calculated in Salchi & Schlickeiser (2004a). The results derived there are also valid for $s > 2$. Therefore we must only determine $D_{\mu\mu}^{\rm T}$ and $A^{\rm T}$, which is done in turn.

3.1. Transit-time damping contribution of fastmode waves A^T

According to Shalchi & Schlickeiser (2004a), the transit-time damping contribution to the pitch-angle Fokker-Planck coefficient is

$$\begin{aligned} D_{\mu\mu}^{\rm T} \;=\; & \frac{2\pi^2\Omega^2(1-\mu^2)}{B_0^2}\sum_{j=\pm1} I_0^j \\ & \times \int_{-1}^{+1} {\rm d}\eta\, \frac{1+\eta^2}{\left[\eta^2 + \Lambda_{\rm F}(1-\eta^2)\right]^{(s_{\rm F}+2)/2}} \\ & \times \int_{k_{\rm min}}^{\infty} {\rm d}k\, k^{-s_{\rm F}} \delta\left[kv\mu\eta - jv_{\rm A}k\right] \left(J'_0(W)\right)^2 \end{aligned} \tag{9}$$

Table 1. Parameters used in the current paper.

Parameter	Symbol
Gyrofrequency	Ω
Pitch-angle cosine	μ
Magnetic background field (mean field)	B_0
Turbulent magnetic field (magnetosonic contribution)	$\delta B_{\rm F}$
Turbulent magnetic field (Alfvénic contribution)	$\delta B_{\rm A}$
Anisotropy parameter of fast mode waves	$\Lambda_{\rm F}$
Anisotropy parameter of shear Alfvén waves	$\Lambda_{\rm A}$
Inertial range spectral index of fast mode waves	$s_{\rm F}$
Inertial range spectral index of shear Alfvén waves	$s_{\rm A}$
Particle velocity	v
Alfvén velocity	$v_{\rm A}$
Small wavenumber cutoff	$k_{\rm min}$
Gyroradius	$R_{\rm L}$

where we used $W = R_{\rm L}k\sqrt{(1-\mu^2)(1-\eta^2)}$. In Table 1 we explain all parameters used in Eq. (9) and the current paper. With

$$I_0 = 2I_0^+ = 2I_0^- = \frac{(s_{\rm F}-1)k_{\rm min}^{s_{\rm F}-1}\delta B_{\rm F}^2}{4\pi J(\Lambda_{\rm F}, s_{\rm F})} \tag{10}$$

and

$$\begin{aligned} J(\Lambda, s) &= {}_2F_1\left(\frac{s+2}{2}, 1, \frac{3}{2}; 1-\Lambda\right) \\ &\approx \begin{cases} \frac{\sqrt{\pi}}{2\Lambda^{(s+1)/2}}\frac{\Gamma((s+1)/2)}{\Gamma((s+2)/2)} & \text{for } \Lambda \ll 1 \\ 1 & \text{for } \Lambda \approx 1 \\ \frac{1}{s\Lambda} & \text{for } \Lambda \gg 1 \end{cases} \end{aligned} \tag{11}$$

and by performing the η-integral, we find, after some straightforward algebra,

$$\begin{aligned} D_{\mu\mu}^T(\mu < \epsilon) &= 0 \\ D_{\mu\mu}^T(\mu \geq \epsilon) &= \frac{\pi(s_{\rm F}-1)vR_{\rm L}^{s_{\rm F}-2}k_{\rm min}^{s_{\rm F}-1}\delta B_{\rm F}^2}{2J(\Lambda_{\rm F}, s_{\rm F})B_0^2} \\ &\quad \times F(\mu, \epsilon, \Lambda_{\rm F}, s_{\rm F}) \cdot G(\mu, R, s_{\rm F}). \end{aligned} \tag{12}$$

Here we define both functions

$$\begin{aligned} F(\mu, \epsilon, \Lambda, s) &= (1-\mu^2)^{1+s/2}\left(1+\frac{\epsilon^2}{\mu^2}\right)\left(1-\frac{\epsilon^2}{\mu^2}\right)^{s/2} \\ &\quad \times \frac{\mu^{s+1}}{\left[\epsilon^2+\Lambda(\mu^2-\epsilon^2)\right]^{(s+2)/2}} \end{aligned} \tag{13}$$

and

$$G(\mu, \epsilon, R, s) = \int_u^\infty {\rm d}x\, x^{-s-1}J_1^2(x), \tag{14}$$

where we use

$$u = R\sqrt{1-\mu^2}\sqrt{1-\frac{\epsilon^2}{\mu^2}}, \tag{15}$$

$R = R_{\rm L}k_{\rm min}$ and $\epsilon = v_{\rm A}/v$. In Appendix A we demonstrate that for $2 < s < 4$ and for $R \ll 1$

$$\begin{aligned} G(\mu, R, s) &\approx \frac{u^{2-s}}{4(s-2)} \\ &= \frac{1}{4(s-2)}R^{2-s}(1-\mu^2)^{(2-s)/2}\left(1-\frac{\epsilon^2}{\mu^2}\right)^{(2-s)/2}. \end{aligned} \tag{16}$$

According to Shalchi & Schlickeiser (2004a) the transit-time contribution to the momentum diffusion coefficient is given by

$$\begin{aligned} A^{\rm T} &= \frac{\pi}{2}(s_{\rm F}-1)\left(\frac{\delta B_{\rm F}}{B_0}\right)^2(k_{\rm min}R_{\rm L})^{s_{\rm F}-1} \\ &\quad \times \frac{v\epsilon^2p^2}{R_{\rm L}}h^{\rm T}(\Lambda_{\rm F}, \epsilon, s_{\rm F}) \end{aligned} \tag{17}$$

with

$$\begin{aligned} h^{\rm T}(\Lambda_{\rm F}, \epsilon, s_{\rm F}) &= \frac{1}{J(\Lambda_{\rm F}, s_{\rm F})} \\ &\quad \times \int_\epsilon^1 {\rm d}\mu\, G(\mu, R, s_{\rm F})F(\mu, \epsilon, \Lambda_{\rm F}, s_{\rm F}). \end{aligned} \tag{18}$$

With Eqs. (13) and (16) this becomes

$$\begin{aligned} h^{\rm T}(\Lambda_{\rm F}, \epsilon, s_{\rm F}) &= \frac{1}{J(\Lambda_{\rm F}, s_{\rm F})}\frac{R^{s_{\rm F}-2}}{4(s_{\rm F}-2)} \\ &\quad \times \int_\epsilon^1 {\rm d}\mu \frac{\mu^{s_{\rm F}-3}(1-\mu^2)^2(\mu^2+\epsilon^2)(\mu^2-\epsilon^2)}{\left[\epsilon^2+\Lambda_{\rm F}(\mu^2-\epsilon^2)\right]^{(s_{\rm F}+2)/2}}. \end{aligned} \tag{19}$$

Defining the integral

$$I_n(\Lambda_{\rm F}, \epsilon, s) = \int_\epsilon^1 {\rm d}\mu \frac{\mu^{s+2n+1}}{\left[\epsilon^2+\Lambda(\mu^2-\epsilon^2)\right]^{(s+2)/2}} \tag{20}$$

and the function

$$I(\Lambda, \epsilon, s) = (1-\epsilon^4)I_0 + I_{+2} - 2I_{+1} - \epsilon^4 I_{-2} + 2\epsilon^4 I_{-1}, \tag{21}$$

the anisotropy function can be rewritten as

$$h^{\rm T}(\Lambda_{\rm F}, \epsilon, s_{\rm F}) = \frac{R^{2-s_{\rm F}}I(\Lambda_{\rm F}, \epsilon, s_{\rm F})}{4(s_{\rm F}-2)J(\Lambda_{\rm F}, s_{\rm F})}. \tag{22}$$

In Appendix B we consider analytical approximations of the integral I_n for different cases. These results can be used to calculate $h^{\rm T}$ for different values of the anisotropy parameter $\Lambda_{\rm F}$ which is done as follows,

3.1.1. Isotropic turbulence $\Lambda_{\rm F} \approx 1$

According to Appendix B we have

$$I_n = \Lambda_{\rm F}^{-s_{\rm F}/2-1} \cdot \begin{cases} \frac{1}{4\epsilon^4} & \text{for } n = -2 \\ \frac{1}{2\epsilon^2} & \text{for } n = -1 \\ \ln\epsilon^{-1} & \text{for } n = 0 \\ \frac{1}{2} & \text{for } n = +1 \\ \frac{1}{4} & \text{for } n = +2 \end{cases}$$

and in combination with Eq. (21) we find

$$I(\Lambda_{\rm F} \approx 1, \epsilon, s_{\rm F}) \approx \Lambda_{\rm F}^{-s_{\rm F}/2-1}\left(\ln\epsilon^{-1} - 1\right). \tag{23}$$

For the nearly isotropic case, we have with $\Delta\Lambda_{\rm F} := 1 - \Lambda_{\rm F} \ll 1$

$$J(\Lambda_{\rm F} \approx 1, s_{\rm F}) = {}_2F_1\left(\frac{s_{\rm F}+2}{2}, 1, \frac{3}{2}; \Delta\Lambda_{\rm F} \ll 1\right) \approx 1 \tag{24}$$

and we obtain for the anisotropy function

$$h^{\rm T}(\Lambda_{\rm F} \approx 1, \epsilon, s_{\rm F}) \approx \frac{R^{2-s_{\rm F}}}{4(s_{\rm F}-2)}\Lambda_{\rm F}^{-s_{\rm F}/2-1}\left(\ln\epsilon^{-1} - 1\right). \tag{25}$$

3.1.2. Strongly parallel turbulence $\Lambda_{\rm F} \gg 1$

Here we have

$$J(\Lambda_{\rm F} \gg 1, s_{\rm F}) \approx \frac{1}{s_{\rm F}\Lambda_{\rm F}} \tag{26}$$

and for the function I_n we have, according to Appendix B,

$$I_n = \frac{1}{s_{\rm F}\Lambda_{\rm F}} \cdot \begin{cases} \frac{1}{\epsilon^4}(1+\frac{s_{\rm F}-4}{s_{\rm F}-2}\frac{1}{\Lambda_{\rm F}}) & \text{for } n=-2 \\ \frac{1}{\epsilon^2}(1+\frac{1}{(s_{\rm F}-2)}\frac{1}{\Lambda_{\rm F}}) & \text{for } n=-1 \\ 1+\frac{s_{\rm F}}{s_{\rm F}-2}\frac{1}{\Lambda_{\rm F}} & \text{for } n=0 \\ \epsilon^2(1+\frac{s_{\rm F}+2}{s_{\rm F}-2}\frac{1}{\Lambda_{\rm F}}) & \text{for } n=+1 \\ \epsilon^4(1+\frac{s_{\rm F}+4}{s_{\rm F}-2}\frac{1}{\Lambda_{\rm F}}) & \text{for } n=+2 \end{cases} \tag{27}$$

and hence

$$I(\Lambda_{\rm F} \gg 1, s_{\rm F}) \approx \frac{4}{s_{\rm F}^2 - 2s_{\rm F}} \frac{1}{\Lambda_{\rm F}^2}. \tag{28}$$

For the anisotropy function, we thus find

$$h^{\rm T}(\Lambda_{\rm F} \gg 1, s_{\rm F}) \approx \frac{R^{2-s_{\rm F}}}{(s_{\rm F}-2)^2\Lambda_{\rm F}}. \tag{29}$$

3.1.3. Strongly perpendicular turbulence $\epsilon^2 \ll \Lambda_{\rm F} \ll 1$

Here we have

$$J(\Lambda_{\rm F} \ll 1, s_{\rm F}) \approx \frac{\sqrt{\pi}}{2\Lambda_{\rm F}^{(s_{\rm F}+1)/2}} \frac{\Gamma(\frac{s_{\rm F}+1}{2})}{\Gamma(\frac{s_{\rm F}+2}{2})} \tag{30}$$

and according to Appendix B

$$I_n = \Lambda_{\rm F}^{-s_{\rm F}/2-1} \times \begin{cases} \frac{\Lambda_{\rm F}^2}{\epsilon^4}(\frac{1}{s_{\rm F}-2}+\frac{1}{4}) & \text{for } n=-2 \\ \frac{\Lambda_{\rm F}}{\epsilon^2}(\frac{1}{s_{\rm F}}+\frac{1}{2}) & \text{for } n=-1 \\ \frac{1}{s_{\rm F}+2}+\ln\epsilon^{-1}+\ln\sqrt{\Lambda_{\rm F}} & \text{for } n=0 \\ \frac{1}{2} & \text{for } n=+1 \\ \frac{1}{4} & \text{for } n=+2 \end{cases} . \tag{31}$$

So we obtain

$$I(\epsilon^2 \ll \Lambda_{\rm F} \ll 1, s_{\rm F}) \approx \frac{\ln\epsilon^{-1} + \ln\sqrt{\Lambda_{\rm F}}}{\Lambda_{\rm F}^{s_{\rm F}/2+1}} \tag{32}$$

and hence

$$h^{\rm T}(\epsilon^2 \ll \Lambda_{\rm F} \ll 1, s_{\rm F}) \approx \frac{\Gamma(\frac{s_{\rm F}+2}{2})}{2\sqrt{\pi}(s_{\rm F}-2)\Gamma(\frac{s_{\rm F}+1}{2})} R^{2-s_{\rm F}} \times \frac{\ln\epsilon^{-1}+\ln\sqrt{\Lambda_{\rm F}}}{\sqrt{\Lambda_{\rm F}}}. \tag{33}$$

3.1.4. Extremely perpendicular turbulence $\Lambda_{\rm F} \ll \epsilon^2 \ll 1$

In this last case we can also apply Eq. (30) but now have

$$I_n(\Lambda_{\rm F} \ll \epsilon^2 \ll 1, s_{\rm F}) \approx \frac{\epsilon^{-s_{\rm F}-2}}{2n+s_{\rm F}+2}. \tag{34}$$

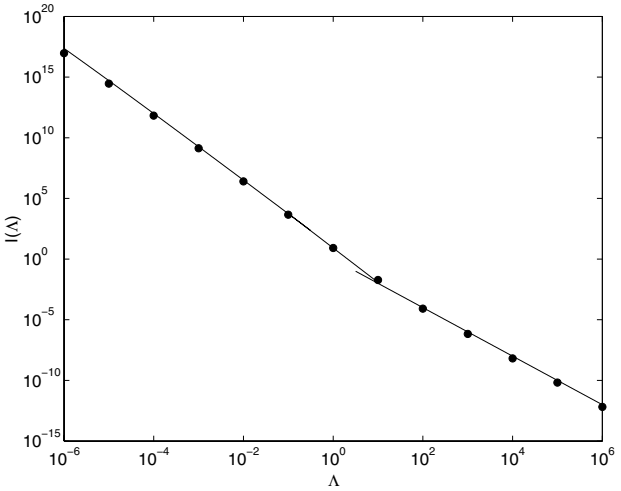

Fig. 1. Analytical (solid lines) and numerical results (dots) of the function $I(\Lambda, \epsilon, s)$ for $s = 2 + 5/3$ and $\epsilon = 10^{-4}$.

In the lowest order to ϵ we find

$$I(\Lambda_{\rm F} \ll \epsilon^2 \ll 1, s_{\rm F}) \approx \frac{8\epsilon^{-s_{\rm F}-2}}{(s_{\rm F}+2)(s_{\rm F}+4)(s_{\rm F}+6)} \tag{35}$$

and for the anisotropy function

$$h^{\rm T}(\Lambda_{\rm F} \ll \epsilon^2 \ll 1, s_{\rm F}) \approx \frac{4\Gamma(\frac{s_{\rm F}+2}{2})R^{2-s_{\rm F}}\Lambda_{\rm F}^{(s_{\rm F}+1)/2}\epsilon^{-s_{\rm F}-2}}{\sqrt{\pi}(s_{\rm F}-2)(s_{\rm F}+2)(s_{\rm F}+4)(s_{\rm F}+6)\Gamma(\frac{s_{\rm F}+1}{2})}. \tag{36}$$

3.1.5. Numerical test of the function $I(\Lambda)$

In Fig. 1 we compare the analytical results of this section for $I(\Lambda, \epsilon, s)$ with numerical results. For this test we assume that $s = 2+5/3$ and $\epsilon = 10^{-4}$. It is obvious that the derived analytical approximations are accurate. Thus the results presented for $h^{\rm T}$ in Sect. 3.1 are reliable for all values of Λ.

3.2. The total momentum diffusion coefficient for fast magnetosonic waves $A^{\rm F}$

The total momentum diffusion coefficient of the fast mode waves $A^{\rm F}$ can be written as a sum of the transit-time-damping contribution $A^{\rm T}$ and the gyroresonance part $A^{\rm G}$. As already discussed in the beginning of Sect. 3, we can use the results of Shalchi & Schlickeiser (2004a) for $A^{\rm G}$:

$$A^{\rm G} = \frac{\pi}{2}(s_{\rm F}-1)\left(\frac{\delta B_{\rm F}}{B_0}\right)^2 R^{s_{\rm F}-1}\frac{v\epsilon^2 p^2}{R_{\rm L}} h^G(\Lambda_{\rm F}, \epsilon, s_{\rm F}) \tag{37}$$

with

$$h^{\rm G}(\Lambda_{\rm F}=1) = \frac{c_2(s_{\rm F})}{(s_{\rm F}+1)2^{(s_{\rm F}-1)/2}}\, {}_2F_1\left(-\frac{1}{2}, \frac{s_{\rm F}+1}{2}; \frac{s_{\rm F}+3}{2}; \frac{1}{2}\right) + \frac{1}{s_{\rm F}}\left[\frac{1}{s_{\rm F}} - \frac{1}{s_{\rm F}+2} - \frac{1}{s_{\rm F}2^{s_{\rm F}/2}} + \frac{1}{(s_{\rm F}+2)2^{(s_{\rm F}+2)/2}}\right],$$

$$h^{\rm G}(\Lambda_{\rm F} \gg 1) = \frac{2}{s_{\rm F}(s_{\rm F}+2)}, h^{\rm G}(\epsilon^{2(s_{\rm F}+1)/s_{\rm F}} \ll \Lambda_{\rm F} \ll 1) = \frac{\zeta(s_{\rm F}+1)}{(s_{\rm F}+2)\sqrt{\pi}}\frac{\Gamma(\frac{s_{\rm F}+1}{2})}{\Gamma(\frac{s_{\rm F}+2}{2})}\Lambda_{\rm F}^{s_{\rm F}/2},$$

$$h^{\rm G}(\Lambda_{\rm F} \ll \epsilon^{2(s_{\rm F}+1)/s_{\rm F}} \ll 1) = \frac{\zeta(s_{\rm F}+1)}{\pi}\epsilon^{s_{\rm F}+1}. \tag{38}$$

The function c_2 was defined in Shalchi & Schlickeiser (2004a, Eq. (22)) as

$$c_2(s) = \frac{2\zeta(s+1)\Gamma\left(\frac{s+3}{2}\right)}{\sqrt{\pi}(s+1)\Gamma\left(\frac{s+2}{2}\right)} = \frac{\zeta(s+1)}{\sqrt{\pi}}\frac{\Gamma(\frac{s+1}{2})}{\Gamma(\frac{s+2}{2})}. \quad (39)$$

We used the Riemann zeta-function $\zeta(x) = \sum_{n=1}^{\infty} n^{-x}$ in the last few equations. Applying $h^{\rm F} = h^{\rm T} + h^{\rm G}$ and neglecting small terms we obtain:

$$h^{\rm F}(\Lambda_{\rm F} = 1) = \frac{R^{2-s_{\rm F}}}{4(s_{\rm F}-2)}(\ln\epsilon^{-1} - 1)$$
$$h^{\rm F}(\Lambda_{\rm F} \gg 1) = \frac{2}{s_{\rm F}(s_{\rm F}+2)} + \frac{R^{2-s_{\rm F}}}{(s_{\rm F}-2)^2\Lambda_{\rm F}}$$
$$h^{\rm F}(\epsilon^2 \ll \Lambda_{\rm F} \ll 1) = \frac{\Gamma(\frac{s_{\rm F}+2}{2})}{2\sqrt{\pi}(s_{\rm F}-2)\Gamma(\frac{s_{\rm F}+1}{2})}R^{2-s_{\rm F}} \times\frac{\ln\epsilon^{-1} + \ln\sqrt{\Lambda_{\rm F}}}{\sqrt{\Lambda_{\rm F}}}. \quad (40)$$

In the isotropic and perpendicular case the transit-time-damping contribution is dominant. For $\Lambda_{\rm F} \gg 1$ both contributions cannot be neglected. This behaviour is different from the flat wave spectrum results presented in Shalchi & Schlickeiser (2004a). In the last subsections we did not consider the case $\Lambda_{\rm F} \ll \epsilon^2 \ll 1$, which is the nearly pure 2D case. For pure 2D geometry the anisotropy function is

$$h^{\rm F}(\Lambda_{\rm F} = 0) = \frac{\zeta(s_{\rm F}+1)}{\pi}\epsilon^{s_{\rm F}+1}. \quad (41)$$

For applications this case shouldn't be important. With Eq. (40) the fast mode momentum diffusion coefficient is given by

$$A^{\rm F} = \frac{\pi}{2}(s_{\rm F}-1)\left(\frac{\delta B_{\rm F}}{B_0}\right)^2 R^{s_{\rm F}-1}\frac{v\epsilon^2 p^2}{R_{\rm L}}h^{\rm F}(R, \Lambda_{\rm F}, \epsilon, s_{\rm F}). \quad (42)$$

3.3. The mixed momentum diffusion coefficient $A^{\rm MIX}$

Here we assume a mixed turbulence model (compare with Shalchi & Schlickeiser 2004a) and equal strength of Alfvén waves and fast magnetosonic waves

$$\delta B := \delta B_{\rm A} \approx \delta B_{\rm F}. \quad (43)$$

Futhermore, we assume that the different cutoff wave numbers are comparable

$$k_{\rm min} := k_{\rm min,A} \approx k_{\rm min,F}. \quad (44)$$

The mixed momentum diffusion coefficient is the sum of the Alfvén and the fast mode coefficient

$$A^{\rm MIX} = A^{\rm A} + A^{\rm F}. \quad (45)$$

With

$$A^{\rm A} = \frac{\pi}{2}(s_{\rm A}-1)\left(\frac{\delta B}{B_0}\right)^2 R^{s_{\rm A}-1}\frac{v\epsilon^2 p^2}{R_{\rm L}}h^{\rm A}(\Lambda_{\rm A}, \epsilon, s_{\rm A}), \quad (46)$$

$$A^{\rm F} = \frac{\pi}{2}(s_{\rm F}-1)\left(\frac{\delta B}{B_0}\right)^2 R^{s_{\rm F}-1}\frac{v\epsilon^2 p^2}{R_{\rm L}}h^{\rm F}(\Lambda_{\rm F}, \epsilon, s_{\rm F}) \quad (47)$$

Table 2. Parameters used for our calculations. The values should be appropriate for the interstellar medium (see Lazar et al. 2003 and Spanier & Schlickeiser 2005). If a parameter is different from these values, we note this separately in the corresponding figures and discussions.

Parameter	Symbol	Value
Spectral index of fast mode waves	$s_{\rm F}$	2.53
Spectral index of Alfvén waves	$s_{\rm A}$	11/3
Anisotropy parameter of fast mode waves	$\Lambda_{\rm F}$	1
Anisotropy parameter of shear Alfvén waves	$\Lambda_{\rm A}$	1
Alfvén speed	$v_{\rm A}$	$10^{-4}c$
Cutoff wavenumber	$k_{\rm min}^{-1}$	2×10^{13} km
Background field	B_0	$0.4nT$
Turbulence strength	$\delta B^2/B_0^2$	0.5

and the function $h^{\rm F}$ given by Eq. (40) and $h^{\rm A}$ given in Teufel et al. (2003, Sect. 4),

$$h^{\rm A}(\Lambda_{\rm A} = 1, s_{\rm A}) \approx \left[\left(\frac{1}{2} + \frac{4\zeta(s_{\rm A}+1)}{\pi}\right)\frac{2^{\frac{-s_{\rm A}+2}{2}}}{s_{\rm A}+2} + \left(\frac{1}{s_{\rm A}} + \frac{1-2^{\frac{2-s_{\rm A}}{2}}}{s_{\rm A}(2-s_{\rm A})}\right)\left(\frac{1-2^{-s_{\rm A}/2}}{s_{\rm A}} + \frac{2^{\frac{-s_{\rm A}+2}{2}}-1}{s_{\rm A}+2}\right)\right],$$
$$h^{\rm A}(\Lambda_{\rm A} \ll 1, s_{\rm A}) \approx \frac{2\Lambda_{\rm A}^{(s_{\rm A}+1)/2}}{\sqrt{\pi}}\frac{\Gamma(\frac{s_{\rm A}+2}{2})}{\Gamma(\frac{s_{\rm A}+1}{2})} \times\left(\frac{1}{2} + \frac{4\zeta(s_{\rm A}+1)}{\pi}\right)\frac{1}{2(s_{\rm A}+2)}\left(1 + \frac{1}{2^{(s_{\rm A}+2)/2}}\right),$$
$$h^{\rm A}(\Lambda_{\rm A} \gg 1, s_{\rm A}) \approx \left[\frac{1}{s_{\rm A}} - \frac{1}{s_{\rm A}+2}\right], \quad (48)$$

the mixed coefficient $A^{\rm MIX}$ can be determined without further problems. The results for shear Alfvén waves are valid for $s < 2$ and $s > 2$. In turn we use these results to calculate $A^{\rm A}$, $A^{\rm F}$, and $A^{\rm MIX}$ for different particles and different turbulence parameters.

3.4. Results for $A^{\rm A}$, $A^{\rm F}$, and $A^{\rm MIX}$

Here we compute the momentum diffusion coefficient for a pure Alfvénic, a pure magnetosonic, and a mixed turbulence model by applying Eqs. (45), (46), and (47) with Eqs. (40) and (48). For the interstellar medium the turbulence parameters shown in Table 2 should be realistic.

To express the particle velocity v by the dimensionless rigidity R, we can use

$$v = c\frac{R}{\sqrt{R_0^2 + R^2}} \quad (49)$$

with the speed of light c and

$$R_0 = \frac{k_{\rm min}}{B_0}\cdot\begin{cases} 0.511MV \text{ for } {\rm e}^- \\ 938MV \text{ for } {\rm p}^+. \end{cases} \quad (50)$$

For the parameters we have for electrons $R_0({\rm e}^-) \approx 2.2\times10^{-10}$ and protons $R_0({\rm p}^+) \approx 0.4\times10^{-6}$.

In order to determine the transport coefficients of the isotropic part of the particle distribution function, we must restrict our calculations to $\epsilon = v_{\rm A}/v \ll 1$ (Schlickeiser 2002).

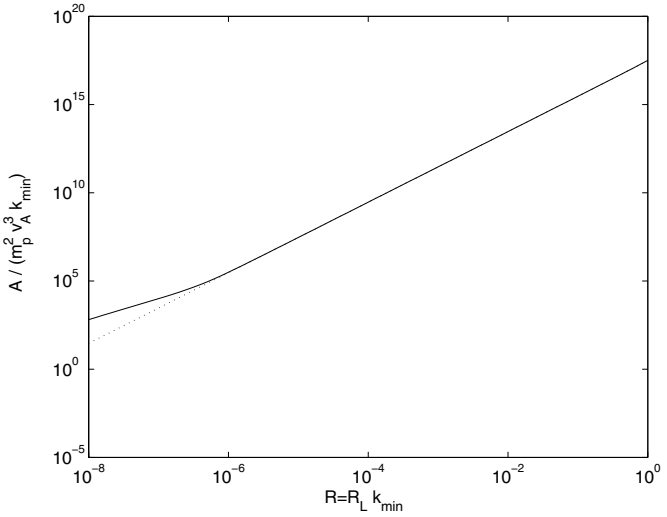

Fig. 2. The momentum diffusion coefficient for electrons (dotted line) and protons (solid line) for isotropic mixed turbulence.

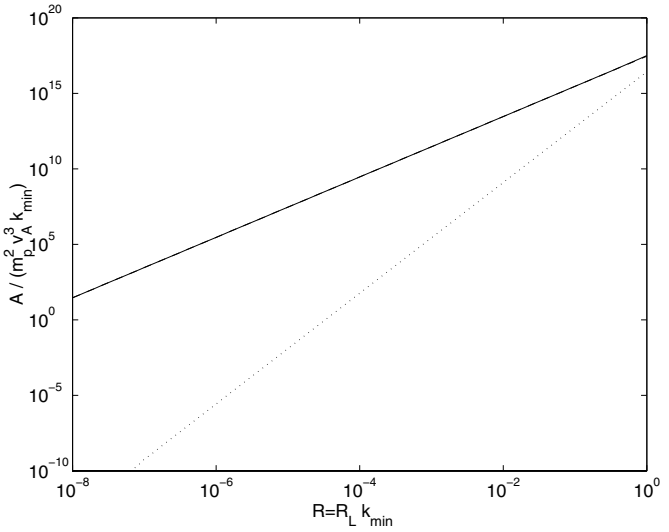

Fig. 3. The momentum diffusion coefficient for electrons for different turbulence models: pure Alfvénic (dotted line), pure magnetosonic (dashed line), and mixed (solid line) turbulence. The dashed and the solid lines are in coincidence.

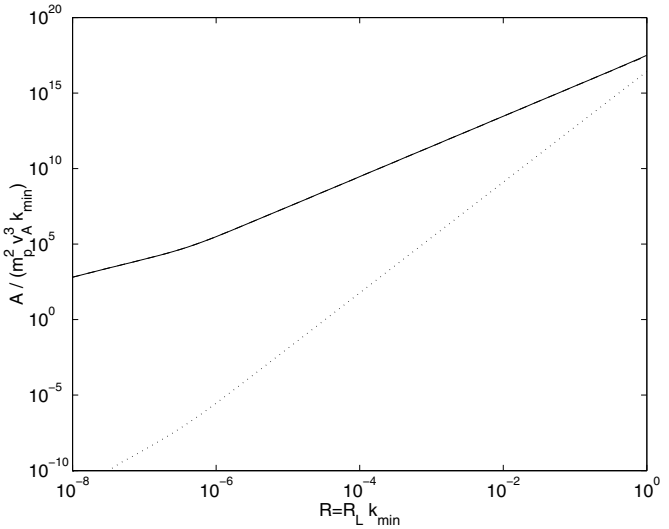

Fig. 4. The momentum diffusion coefficient for protons for different turbulence models: pure Alfvénic (dotted line), pure magnetosonic (dashed line), and mixed (solid line) turbulence. The dashed and the solid lines are in coincidence.

Thus, we can only consider rigidities that satisfy the following condition:

$$R \gg \frac{R_0}{\sqrt{(c/v_\mathrm{A})^2 - 1}} \approx R_0 \frac{v_\mathrm{A}}{c}. \tag{51}$$

For $v_\mathrm{A} = 10^{-4}c$ we find the restriction $R(\mathrm{e}^-) \gg 2.2 \times 10^{-14}$ for electrons and $R(\mathrm{p}^+) \gg 0.4 \times 10^{-10}$ for protons. On the other hand, all formulas derived in this paper are restricted to $R = R_\mathrm{L} k_\mathrm{min} \ll 1$. Therefore we only consider a parameter regime of $10^{-8} \leq R \leq 10^0$ for all the following discussions. We calculate the dimensionless momentum diffusion coefficient

$$\tilde{A}^i = \frac{A^i}{m_\mathrm{p}^2 v_\mathrm{A}^3 k_\mathrm{min}} \tag{52}$$

with the proton mass m_p.

Figure 2 shows the mixed momentum diffusion coefficient A^MIX as a function of the dimensionless rigidity R for electrons and protons and for $\Lambda_\mathrm{A} = \Lambda_\mathrm{F} = 1$. Only for non-relativistic protons ($R \leq R_0(\mathrm{p}^+)$) do we find a different momentum diffusion coefficient for the different particles. In the relativistic range ($R \geq R_0(\mathrm{p}^+) > R_0(\mathrm{e}^-)$), both results are in coincidence and the rigidity dependence is approximately $A \sim R^2$. In comparison to diffusion coefficients calculated for the Kolmogorov spectrum ($s_\mathrm{A} = s_\mathrm{F} = 5/3$), the rigidity dependence is steeper. To compute the coefficients shown in Fig. 2, we assumed isotropic ($\Lambda_\mathrm{A} = \Lambda_\mathrm{F} = 1$) and mixed turbulence. In Figs. 3 and 4 we have shown results for the same parameters but considered pure Alfvénic, pure magnetosonic, and mixed turbulence for electrons and protons. For both particles the magnetosonic and mixed results are in coincidence. Obviously the mixed momentum diffusion coefficient is controlled by the fast mode waves. The results for pure Alfvénic turbulence is even steeper than in the mixed model. The domination of fast magnetosonic waves occurs because the transit-time contribution is always larger than the gyroresonance contribution.

4. Parallel spatial diffusion coefficients for a steep wave spectrum

According to Jokipii (1966), Hasselmann & Wibberenz (1968), and Earl (1974), the parallel mean free path results from the pitch-angle-cosine average of the inverse pitch-angle Fokker-Planck coefficient $D_{\mu\mu}$ as

$$\begin{aligned}\lambda_\parallel &= \frac{3}{v}\kappa_\parallel = \frac{3v}{8}\int_{-1}^{+1} \mathrm{d}\mu \frac{(1-\mu^2)^2}{D_{\mu\mu}} \\ &= \frac{3v}{4}\int_0^1 \mathrm{d}\mu \frac{(1-\mu^2)^2}{D_{\mu\mu}}\end{aligned} \tag{53}$$

where we again used that $D_{\mu\mu}$ is symmetric in μ. Alternatively, the parallel spatial diffusion coefficient $\kappa_\parallel$ can be calculated. With the results of Sect. 3 for $D^T_{\mu\mu}$ and with the coefficients $D^G_{\mu\mu}$ and $D^A_{\mu\mu}$ calculated in Teufel et al. (2003) and

Shalchi & Schlickeiser (2004a), it is straightforward to compute the coefficients

$$\lambda_\parallel^A \approx \frac{3v}{4}\int_0^\epsilon \mathrm{d}\mu \frac{(1-\mu^2)^2}{D_{\mu\mu}^A(\mu\ll\epsilon)} + \frac{v^2}{4}\int_\epsilon^1 \mathrm{d}\mu \frac{(1-\mu^2)^2}{D_{\mu\mu}^A(\mu\gg\epsilon)}$$

$$\lambda_\parallel^F \approx \frac{3v}{4}\int_0^\epsilon \mathrm{d}\mu \frac{(1-\mu^2)^2}{D_{\mu\mu}^G(\mu\ll\epsilon)} + \frac{v^2}{4}\int_\epsilon^1 \mathrm{d}\mu \frac{(1-\mu^2)^2}{D_{\mu\mu}^{\mathrm{G}}(\mu\gg\epsilon)+D_{\mu\mu}^{\mathrm{T}}(\mu\gg\epsilon)}$$

$$\lambda_\parallel^{\mathrm{MIX}} \approx \frac{3v}{4}\int_0^\epsilon \mathrm{d}\mu \frac{1}{D_{\mu\mu}^{\mathrm{G}}(\mu\ll\epsilon)+D_{\mu\mu}^{\mathrm{A}}(\mu\ll\epsilon)} + \frac{v^2}{4}\int_\epsilon^1 \mathrm{d}\mu \frac{(1-\mu^2)}{D_{\mu\mu}^{\mathrm{G}}(\mu\gg\epsilon)+D_{\mu\mu}^{A}(\mu\gg\epsilon)+D_{\mu\mu}^{\mathrm{T}}(\mu\geq\epsilon)} \tag{54}$$

by performing the μ-integration numerically. For the pitch-angle Fokker-Planck coefficients, we have (see Sect. 3; and Teufel et al. 2003)

$$\begin{aligned}
D_{\mu\mu}^{\mathrm{T}}(\mu<\epsilon) &= 0\\
D_{\mu\mu}^{\mathrm{T}}(\mu\geq\epsilon) &= \frac{\pi(s_{\mathrm{F}}-1)vR_{\mathrm{L}}^{s_{\mathrm{F}}-2}k_{\mathrm{min}}^{s_{\mathrm{F}}-1}\delta B^2}{2J(\Lambda_{\mathrm{F}},s_{\mathrm{F}})B_0^2}\\
&\quad\times F(\mu,\epsilon,\Lambda_{\mathrm{F}},s_{\mathrm{F}})\cdot G(\mu,\epsilon,R,s_{\mathrm{F}})\\
D_{\mu\mu}^{\mathrm{G}}(\mu\ll\epsilon) &= \frac{\pi(s_{\mathrm{F}}-1)vR_{\mathrm{L}}^{s_{\mathrm{F}}-2}k_{\mathrm{min}}^{s_{\mathrm{F}}-1}\delta B^2}{2J(\Lambda_{\mathrm{F}},s_{\mathrm{F}})B_0^2}\\
&\quad\times\epsilon^{s_{\mathrm{F}}-1}\cdot W_{\mathrm{s}}^{G}(\Lambda_{\mathrm{F}},\epsilon,s_{\mathrm{F}})\\
D_{\mu\mu}^{\mathrm{G}}(\mu\gg\epsilon) &= \frac{\pi(s_{\mathrm{F}}-1)vR_{\mathrm{L}}^{s_{\mathrm{F}}-2}k_{\mathrm{min}}^{s_{\mathrm{F}}-1}\delta B^2}{2J(\Lambda_{\mathrm{F}},s_{\mathrm{F}})B_0^2}\\
&\quad\times\mu^{s_{\mathrm{F}}-1}(1-\mu^2)\cdot W_l^{G}(\Lambda_{\mathrm{F}},\mu,s_{\mathrm{F}})\\
D_{\mu\mu}^{\mathrm{A}}(\mu\ll\epsilon) &= \frac{\pi(s_{\mathrm{A}}-1)vR_{\mathrm{L}}^{s_{\mathrm{A}}-2}k_{\mathrm{min}}^{s_{\mathrm{A}}-1}\delta B^2}{2J(\Lambda_{\mathrm{A}},s_{\mathrm{A}})B_0^2}\\
&\quad\times\epsilon^{s_{\mathrm{A}}-1}\cdot W_{\mathrm{s}}^{A}(\Lambda_{\mathrm{A}},\epsilon,s_{\mathrm{A}})\\
D_{\mu\mu}^{\mathrm{A}}(\mu\gg\epsilon) &= \frac{\pi(s_{\mathrm{A}}-1)vR_{\mathrm{L}}^{s_{\mathrm{A}}-2}k_{\mathrm{min}}^{s_{\mathrm{A}}-1}\delta B^2}{2J(\Lambda_{\mathrm{A}},s_{\mathrm{A}})B_0^2}\\
&\quad\times\mu^{s_{\mathrm{A}}-1}(1-\mu^2)\cdot W_l^{\mathrm{A}}(\Lambda_{\mathrm{A}},\mu,s_{\mathrm{A}}).
\end{aligned}\tag{55}$$

Here the functions

$$W_{\mathrm{s}}^{\mathrm{A}}(\Lambda_{\mathrm{A}},\epsilon,s_{\mathrm{A}}) \simeq \begin{cases} \frac{1}{s_{\mathrm{A}}\Lambda_{\mathrm{A}}\epsilon^2} & \text{for} \quad \Lambda_{\mathrm{A}}\epsilon^2 \gg 1\\ \frac{1}{2}+\frac{4\zeta(s_{\mathrm{A}}+1)}{\pi} & \text{for} \quad \Lambda_{\mathrm{A}}\epsilon^2 \ll 1 \end{cases} \tag{56}$$

$$W_l^{\mathrm{A}}(\Lambda_{\mathrm{A}},M,s_{\mathrm{A}}) \simeq \begin{cases} \frac{M^2}{s_{\mathrm{A}}\Lambda_{\mathrm{A}}}\left[1+\frac{1-(1+\Lambda_{\mathrm{A}})^{\frac{2-s_{\mathrm{A}}}{2}}}{(2-s_{\mathrm{A}})\Lambda_{\mathrm{A}}}\right] & \text{for } M^2\ll 1, M^2\ll\Lambda_{\mathrm{A}}\\ \frac{1}{4}+\frac{2\zeta(s_{\mathrm{A}}+1)}{\pi} & \text{for} \quad \Lambda_{\mathrm{A}}\ll M^2\ll 1\\ \frac{M^2}{s_{\mathrm{A}}\Lambda_{\mathrm{A}}} & \text{for} \quad 1\ll M^2\ll\Lambda_{\mathrm{A}}\\ \frac{1}{2}+\frac{4\zeta(s_{\mathrm{A}}+1)}{\pi} & \text{for} \quad M^2\gg 1, M^2\gg\Lambda_{\mathrm{A}} \end{cases} \tag{57}$$

$$W_{\mathrm{s}}^{\mathrm{G}}(\Lambda_{\mathrm{F}},\epsilon,s_{\mathrm{F}}) \simeq \begin{cases} \frac{c_2\epsilon}{2\Lambda_{\mathrm{F}}^{(s_{\mathrm{F}}+1)/2}} & \text{for} \quad \Lambda_{\mathrm{F}}\ll 1\\ \frac{3\zeta(s_{\mathrm{F}}+1)\epsilon}{4} & \text{for} \quad \Lambda_{\mathrm{F}}=1\\ \frac{c_2\epsilon}{\sqrt{\Lambda_{\mathrm{F}}}} & \text{for} \quad \epsilon^{-2}\gg\Lambda_{\mathrm{F}}\gg 1\\ \frac{1}{2s_{\mathrm{F}}\Lambda_{\mathrm{F}}} & \text{for} \quad \Lambda_{\mathrm{F}}\gg\epsilon^{-2}\gg 1 \end{cases} \tag{58}$$

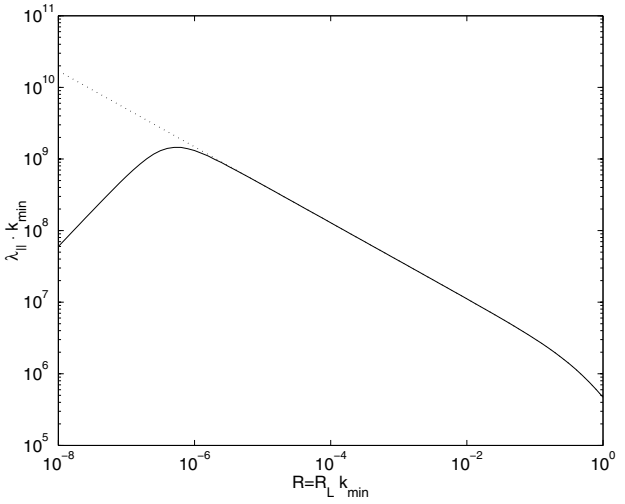

Fig. 5. The parallel mean free path for electrons (dotted line) and protons (solid line) for isotropic mixed turbulence.

and

$$W_l^{\mathrm{G}}(\Lambda_{\mathrm{F}},M,s_{\mathrm{F}}) \simeq \begin{cases} \frac{1}{s_{\mathrm{F}}\Lambda_{\mathrm{F}}} & \text{for} \quad M^2\ll\Lambda_{\mathrm{F}}\\ \frac{c_2}{M\sqrt{\Lambda_{\mathrm{F}}}} & \text{for} \quad \Lambda_{\mathrm{F}}\ll M^2\ll 1\\ \frac{2c_2}{M\sqrt{\Lambda_{\mathrm{F}}}} & \text{for} \quad \Lambda_{\mathrm{F}}\ll M^2, M^2\gg 1 \end{cases} \tag{59}$$

are used. In turn we use these formulas to compute $\lambda_\parallel^{\mathrm{A}}$, $\lambda_\parallel^{\mathrm{F}}$, and $\lambda_\parallel^{\mathrm{MIX}}$ for different parameters by performing the μ-integrals in Eq. (54) numerically.

4.1. Numerical results for $\lambda_\parallel{}^{\mathrm{A}}$, $\lambda_\parallel{}^{\mathrm{F}}$ and $\lambda_\parallel{}^{\mathrm{MIX}}$

Here we compute the parallel mean free path for a pure Alfvénic, a pure magnetosonic, and for a mixed turbulence model by applying Eqs. (54)–(59) numerically for the interstellar turbulence parameters of Table 2. Calculated is the dimensionless parallel mean free path defined as

$$\tilde{\lambda}_\parallel^i = \lambda_\parallel^i \cdot k_{\mathrm{min}}. \tag{60}$$

Figure 5 shows the mixed parallel mean free path $\lambda_\parallel^{\mathrm{MIX}}$ as a function of the dimensionless rigidity R for electrons and protons and for $\Lambda_{\mathrm{A}}=\Lambda_{\mathrm{F}}=1$. Only for non-relativistic protons ($R\leq R_0(\mathrm{p}^+)$) do we find a difference between the two different particles. In the relativistic range ($R\geq R_0(p^+)>R_0(\mathrm{e}^-)$), we find a decreasing parallel mean free path in contrast to the Kolmogorov results presented in the previous papers. The rigidity dependence is $\lambda_\parallel^{\mathrm{MIX}}\sim R^{-0.53}\sim R^{2-s_{\mathrm{F}}}$, which proves the assumption that the parallel mean free path is controlled by the fast mode contribution. In Figs. 6 and 7 we have shown the parallel mean free path for different values of the fast mode anisotropy parameter Λ_{F}. It seems that variation in Λ_{F} only changes the magnitude of the parallel mean free path but not the rigidity dependence. In Figs. 8 and 9 we explore the parallel mean free path for the three different turbulence models (Alfvénic, magnetosonic, and mixed turbulence). For nearly all rigidities the magnetosonic and mixed results are in coincidence. Thus, the Alfvénic contribution can be neglected in the mixed model. For pure Alfvénic turbulence, the rigidity dependence in the relativistic range is $\lambda_\parallel\sim R^{-1.7}\sim R^{2-s_{\mathrm{A}}}$ as expected. Surprisingly we find a constant parallel mean free path for non-relativistic protons (see dotted line in Fig. 9) and an

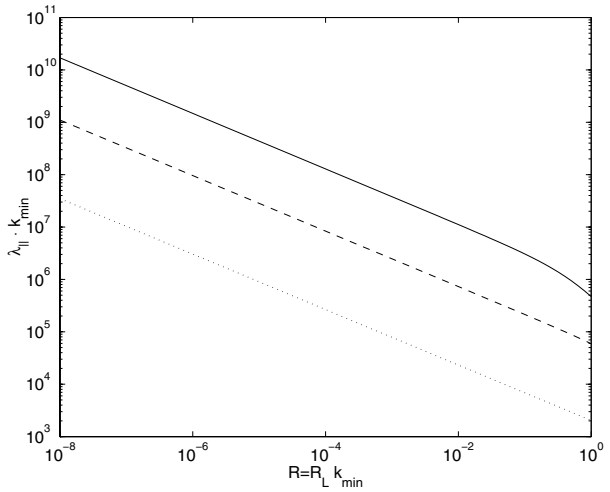

Fig. 6. The parallel mean free path for electrons for different values of the fast magnetosonic Anisotropy parameter: $\Lambda^F = 10^0$ (solid line), $\Lambda^F = 10^2$ (dashed line), and $\Lambda^F = 10^5$ (dotted line).

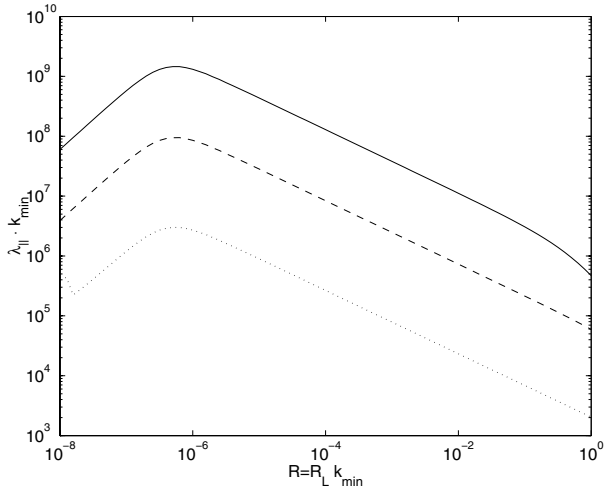

Fig. 7. The parallel mean free path for protons for different values of the fast magnetosonic Anisotropy parameter: $\Lambda^F = 10^0$ (solid line), $\Lambda^F = 10^2$ (dashed line), and $\Lambda^F = 10^5$ (dotted line).

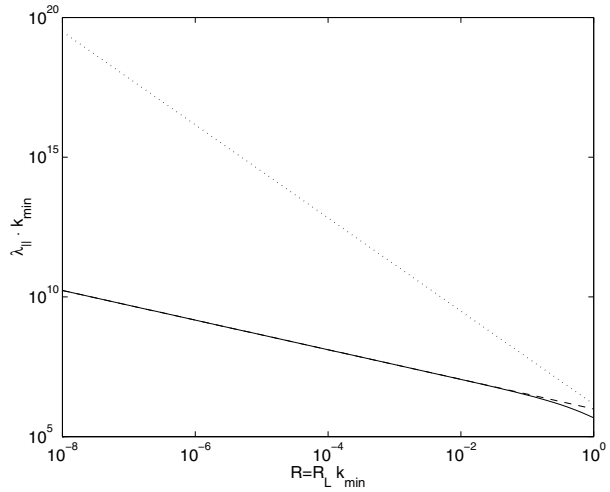

Fig. 8. The parallel mean free path for electrons for different turbulence models: pure Alfvénic (dotted line), pure magnetosonic (dashed line), and mixed (solid line) turbulence.

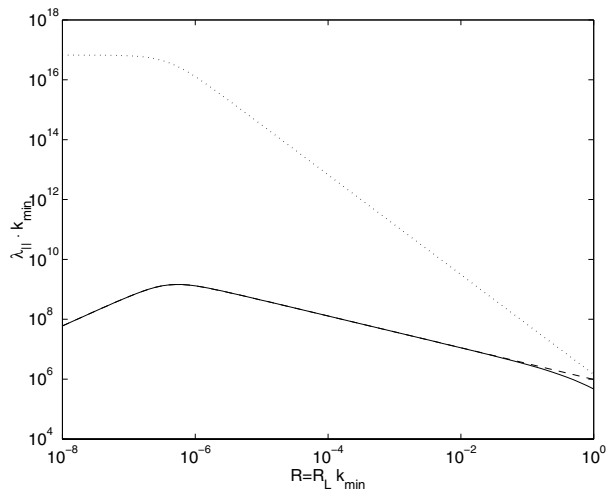

Fig. 9. The parallel mean free path for protons for different turbulence models: pure Alfvénic (dotted line), pure magnetosonic (dashed line), and mixed (solid line) turbulence.

increasing parallel mean free path for non-relativistic electrons (see solid line in Fig. 9).

5. Nonlinear effects in cosmic-ray transport theory

In the current paper we have employed quasilinear theory to calculate diffusion coefficients. While it is accepted that QLT is unable to describe perpendicular diffusion (see e.g. Shalchi & Schlickeiser 2004b), it has been assumed for a long time that QLT is correct for parallel transport. By comparing QLT with numerical test particle simulations (e.g. Qin et al. 2002a,b; Qin et al. 2006), it was noticed that there are two problems of QLT if the parallel mean free path is calculated:

5.1. The 90°-problem

QLT is problematic for pitch-angle scattering close to 90° (see Völk 1973; Jones et al. 1973; Owens 1974; Völk 1975; Goldstein 1976; Jones et al. 1978; Shalchi 2005). We expect that for momentum diffusion the small-μ behaviour of the pitch-angle Fokker-Planck coefficient is insignificant and hence QLT should be valid. Therefore the results presented for momentum diffusion in this paper should be accurate. For parallel diffusion and a steep wave spectrum, $D_{\mu\mu}$ at low values of μ controls the parallel mean free path. Because QLT is incorrect at 90° in a magnetostatic model, one could draw the conclusion that QLT is also incorrect in the plasma-wave model (e.g. for Alfvénic or magnetosonic turbulence), which has been applied in the current paper. The only argument that can defend the results presented in this paper is that plasma-wave propagation effects suppress nonlinear effects and QLT is recovered. Because all simulations and nonlinear calculations were done in a magnetostatic model, it is prematurely to make a decision about whether the results for parallel spatial diffusion presented here are accurate or not. It is a project in our future work to consider pitch-angle diffusion in dynamical and plasma-wave turbulence within the recently derived second order QLT (SOQLT, Shalchi 2005). Only such calculations could give us a hint whether QLT is correct for parallel diffusion and steep wave spectra within the plasma-wave model. An alternative method for testing the validity of quasilinear diffusion coefficients would be a comparison with numerical test particle simulations. In the near future such simulations should be done within different plasma-wave models and for steep spectra.

5.2. The geometry problem

As noted in recent papers (Minnie 2002; Qin 2002; Shalchi et al. 2004a; Qin et al. 2006), QLT also becomes more and more inaccurate if we merge from pure slab geometry ($\Lambda = \infty$) to pure 2D geometry ($\Lambda = 0$). In non-slab models perpendicular transport itself causes resonance broadening, and the parallel mean free path becomes smaller due to this resonance broadening effect. Thus, a nonlinear description of parallel diffusion in non-slab models seems to be more appropriate (see Shalchi et al. 2004a). Therefore the results of the current paper are only correct for certain parameter regimes, e.g. for weak turbulence ($\delta B \ll B_0$) or for more parallel oriented turbulence ($\Lambda \geq 1$). So far only the weakly nonlinear theory (WNLT, Shalchi et al. 2004a) is able to describe parallel transport in agreement with test particle simulations for slab/2D composite geometry. But the theory has so far not been applied to isotropic or anisotropic turbulence models because of mathematical problems. Therefore it is not clear how important nonlinear effects are for isotropic turbulence, which was considered in most of the discussions in this paper. Furthermore, one could assume that plasma-wave effects can supress nonlinear effects and that QLT could be recovered in this case. But the recovery of QLT in more realistic turbulence models (non-magnetostatic models) has not been proved so far. It should be a project in future work to consider parallel spatial diffusion in dynamical and plasma-wave turbulence within WNLT.

6. Summary and conclusions

In Lazar et al. (2003) and Spanier & Schlickeiser (2005), a steep wave spectrum ($s > 2$) in the inertial range was proposed. For such a steep wave spectrum, we calculated the quasilinear momentum diffusion coefficient and the quasilinear parallel mean free path by assuming the turbulence parameters of the interstellar medium. We obtained the following results:

1. The momentum diffusion coefficient in the mixed model is controlled by the magnetosonic contribution.
2. For relativistic particles the electron and proton results are in coincidence. We find $A \sim R^2$ behaviour of the momentum diffusion coefficient. If a pure Alfvénic turbulence is realized in the ISM, the rigidity dependence is even steeper.
3. The parallel mean free path decreases with increasing rigidities in the relativistic range.
4. Relativistic electrons and protons have the same parallel mean free path, but for non-relativistic particles we find quite different results for parallel diffusion.
5. In the mixed model, $\lambda_\parallel$ is controlled by the magnetosonic contribution. The parameter Λ_F only changes the magnitude of $\lambda_\parallel$, not the rigidity dependence.
6. For non-relativistic protons we find an increasing parallel mean free path in the mixed model and a constant parallel mean free path for pure shear Alfvén waves.

Obviously the spectral index has a strong influence on diffusion coefficients. In the case of $s > 2$, we find unexpected behaviour for the parallel mean free path: for very steep spectra $\lambda_\parallel$ decreases with increasing rigidity R.

Because most of the wave power for steep spectra sits at small wavenumbers, high-energy cosmic ray particles are better confined than low-energy cosmic rays, explaining why $\lambda_\parallel$ decreases with energy. It is interesting to explore whether this better confinement of high-energy cosmic ray particles also holds for the propagation of ultra high-energy cosmic rays above the knee ($E > E_K$), which requires extending our analysis to the opposite limit $R_L k_{min} \gg 1$. Such an analysis is most important for a galactic origin of ultra high-energy cosmic rays.

To explore such high rigidities, resonance-broadening effects can no longer be neglected. Therefore plasma-wave damping effects (see e.g. Schlickeiser & Achatz 1993) and dynamical turbulence effects (see e.g. Shalchi et al. 2006) have to be included. In the case of damped plasma-wave turbulence, diffusion coefficients would become dependent of the plasma-β. Futhermore, resonance broadening due to the nonlinear motion of the particle could become important. Therefore nonlinear diffusion theories have to be preferred over the traditional quasilinear approach if the case $R_L k_{min} \gg 1$ is considered.

The mean free path decreasing with rigidity is at odds with the standard interpretation of the measured secondary-primary ratio in galactic cosmic rays. According to Swordy et al. (1990), the observed ratio of secondary to primary cosmic-ray nuclei indicates that the rigidity dependence of the parallel mean free path should be $\lambda_\parallel \sim R^{0.6}$. A possible explanation for this law has already been provided in Shalchi & Schlickeiser (2005), where the weakly nonlinear theory was applied instead of QLT, together with the Kolmogorov magnetic fluctuation spectrum. But a Kolmogorov spectrum for the magnetic fluctuations disagrees with the conclusions of Lazar et al. (2003) and Spanier & Schlickeiser (2005). It seems to us that the theory of galactic cosmic ray propagation is still far from complete.

Acknowledgements. This work was supported by the Deutsche Forschungsgemeinschaft through Sonderforschungsbereich 591.

References

Abramowitz, M., & Stegun, I. A. 1972, Handbook of Mathematical Functions (New York: Dover Publications)
Armstrong, J. W., Rickett, B. J., & Spangler, S. R. 1995, ApJ, 443, 209
Denskat, K. U., & Neubauer, F. M. 1982, JGR, 87, 2215
Dogan, A., Spanier, F., Vainio, R., & Schlickeiser, R. 2005, J. Plasma Physics, in press
Earl, J. A. 1974, ApJ, 193, 231
Goldstein, M. L. 1976, ApJ, 204, 900
Gradshteyn, I. S., & Ryzhik, I. M. 2000, Table of Integrals, Series, and Products (New York: Academic Press)
Hasselmann, K., & Wibberenz, G. 1968, Z. Geophys., 34, 353
Jokipii, J. R. 1966, ApJ, 146, 480
Jones, F. C., Birmingham, T. J., & Kaiser, T. B. 1973, ApJ, 180, L139
Jones, F. C., Birmingham, T. J., & Kaiser, T. B. 1978, Phys. Fluids, 21, 347
Kolmogorov, A. N. 1941, Dokl. Akad. Nauk. SSSR, 30, 301
Kraichnan, R. 1965, Phys. Fluids, 8, 1835
Lazar, M., Spanier, F., & Schlickeiser, R. 2003, A&A, 410, 415
Lerche, I., & Schlickeiser, R. 2001, A&A, 378, 279
Lerche, I., Spanier, F., & Schlickeiser, R. 2005, A&A, submitted
Minnie, J., Master thesis, University of Potchefstroom, South Africa, 2002
Owens, A. J. 1974, ApJ, 191, 235
Qin, G., Ph.D. thesis, University of Delaware, USA, 2002
Qin, G., Matthaeus, W. H., & Bieber, J. W. 2002a, Geophys. Res. Lett., 29
Qin, G., Matthaeus, W. H., & Bieber, J. W. 2002b, ApJ, 578, L117
Qin, G., Matthaeus, W. H., & Bieber, J. W. 2006, ApJ, 640, L103
Schlickeiser, R. 2002, Cosmic Ray Astrophysics (Berlin, Heidelberg: Springer-Verlag)
Schlickeiser, R., & Achatz, U. 1993, J. Plasma Phys., 49, 63
Schlickeiser, R., & Lerche, I. 2002, J. Plasma Phys., 68, 191
Shalchi, A. 2005, Phys. Plasmas, 12, 052905
Shalchi, A., & Schlickeiser, R. 2004a, A&A, 420, 799
Shalchi, A., & Schlickeiser, R. 2004b, A&A, 420, 821
Shalchi, A., & Schlickeiser, R. 2005, ApJ, 626, L97
Shalchi, A., Bieber, J. W., Matthaeus, W. H., & Qin, G. 2004, ApJ, 616, 617
Shalchi, A., Bieber, J. W., Matthaeus, W. H., & Schlickeiser, R. 2006, ApJ, 642, 230
Spanier, F., & Schlickeiser, R. 2005, A&A, 436, 9
Swordy, S. P., et al. 1990, ApJ, 349, 625
Teufel, A., Lerche, I., & Schlickeiser, R. 2003, A&A, 397, 777
Völk, H. J. 1973, Ap&SS, 25, 471
Völk, H. J. 1975, Rev. Geophys. Space Phys., 13, 547
Yan, H., & Lazarian, A. 2004, ApJ, 614, 757

Online Material

Appendix A: The function $G(\mu, R, s)$

Here we investigate the integral

$$G(\mu, R, s) = \int_u^\infty \mathrm{d}x\; x^{-s-1} J_1^2(x). \tag{A.1}$$

By applying

$$J_1(x) = -J_0^{'}(x) \tag{A.2}$$

and

$$J_0^{''}(x) + \frac{1}{x} J_0^{'}(x) + J_0 = 0, \tag{A.3}$$

we find

$$J_1^2(x) = -\frac{x}{2}\frac{\mathrm{d}}{\mathrm{d}x}(J_0^2(x) + J_1^2(x)). \tag{A.4}$$

Therefore the integral can be written as

$$G(u) = -\frac{1}{2}\int_u^\infty \mathrm{d}x\; x^{-s}\frac{\mathrm{d}}{\mathrm{d}x}(J_0^2(x) + J_1^2(x)), \tag{A.5}$$

and after some basic manipulations we find

$$G(u) = \frac{1}{2}u^{-s}\left[J_0^2(u) + J_1^2(u)\right] - \frac{s}{2}G(u) - \frac{s}{2}H(u) \tag{A.6}$$

with the new integral

$$H(u) = \int_u^\infty \mathrm{d}x\; x^{-s-1} J_0^2(x). \tag{A.7}$$

To proceed we apply

$$\sum_{k=-\infty}^{+\infty} J_k^2(x) = 1, \tag{A.8}$$

and hence

$$\begin{aligned} H(u) &= \int_u^\infty \mathrm{d}x\; x^{-s-1} - 2\int_0^\infty \mathrm{d}x\; x^{-s-1} J_1^2(x) \\ &\quad - 2\sum_{k=2}^\infty \int_u^\infty \mathrm{d}x\; x^{-s-1} J_k^2(x) \\ &= \frac{1}{s}u^{-s} - 2G(u) - 2\sum_{k=2}^\infty \int_0^\infty \mathrm{d}x\; x^{-s-1} J_k^2(x). \end{aligned} \tag{A.9}$$

Finally we find the (exact) result

$$\begin{aligned} G(u) &= \frac{u^{-s}}{s-2}\left[1 - J_0^2(u) - J_1^2(u)\right] \\ &\quad + \frac{2s}{2-s}\sum_{k=2}^\infty \int_u^\infty \mathrm{d}x\; x^{-s-1} J_k^2(x). \end{aligned} \tag{A.10}$$

If we restrict our calculations to small rigidities $R \ll 1$, the parameter u is also small. For $u \ll 1$ we obtain

$$\begin{aligned} J_0^2(u) &\approx 1 - \frac{u^2}{2} \\ J_1^2(u) &\approx \frac{u^2}{4} \end{aligned} \tag{A.11}$$

and, therefore,

$$G(u) \approx \frac{u^{2-s}}{4(s-2)} + c_1(s) \tag{A.12}$$

with

$$c_1(s) = \frac{2s}{2-s}\sum_{k=2}^\infty \int_0^\infty \mathrm{d}x\; x^{-s-1} J_k^2(x). \tag{A.13}$$

To obtain this equation we approximate the parameter u by 0. This lowest order approximation can only be performed if $s < 4$. According to Gradshteyn & Ryzhik (2000) we find

$$c_1(s) = \frac{2}{(2-s)s\sqrt{\pi}}\frac{\Gamma(2-\frac{s}{2})\Gamma(\frac{s+1}{2})}{\Gamma(2+\frac{s}{2})\Gamma(\frac{s}{2})}. \tag{A.14}$$

By applying the duplication formula (Abramowitz & Stegun 1974)

$$\Gamma(2z) = \frac{1}{\sqrt{2\pi}} 2^{2z-1/2}\Gamma(z)\Gamma\left(z+\frac{1}{2}\right), \tag{A.15}$$

we find

$$\Gamma\left(\frac{s+1}{2}\right) = \frac{\sqrt{\pi}}{2^s}\frac{\Gamma(s+1)}{\Gamma(\frac{s}{2}+1)}. \tag{A.16}$$

Then the function $G(u)$ can be approximated by

$$G(u \ll 1) \approx \frac{u^{2-s}}{4(s-2)} + \frac{2^{1-s}s}{4-s^2}\frac{\Gamma(s)\Gamma(2-\frac{s}{2})}{\Gamma^3(1+\frac{s}{2})}. \tag{A.17}$$

In turn we consider three different values for the spectral index s, as follows.

A.1. A flat wave spectrum $s < 2$

Here the second term in Eq. (A.17) is dominant, and one gets

$$G(u \ll 1, s < 2) \approx \frac{2^{1-s}s}{4-s^2}\frac{\Gamma(s)\Gamma(2-\frac{s}{2})}{\Gamma^3(1+\frac{s}{2})}, \tag{A.18}$$

which is exactly equal to the formula derived in Shalchi & Schlickeiser (2004a) in a different manner.

A.2. A steep wave spectrum $2 < s < 4$

In this case the first term in Eq. (A.17) is dominant, and we obtain

$$G(u \ll 1) \approx \frac{u^{2-s}}{4(s-2)}. \tag{A.19}$$

This result, which is the most interesting case for the current paper, is quite different from Eq. (A.18). In Sects. 3 and 4 we use this formula to calculate the transit-time-damping contribution to the pitch-angle Fokker-Planck coefficient, which controls the momentum diffusion coefficient and the parallel mean free path.

A.3. A spectrum with $s = 2$

From Eq. (A.17) one could draw the conclusion that the function $G(u)$ is infinity for $s = 2$. Here we demonstrate that this is not correct, so only the derived formula is not applicable in this case. For $s = 2$ we have

$$G(u \ll 1, s = 2) = \int_u^\infty \frac{\mathrm{d}x}{x^3} J_1^2(x). \tag{A.20}$$

It is obvious that the main contribution to the integral comes from low values of x. Therefore we split the integral

$$G(u \ll 1, s = 2) = \int_u^1 \frac{\mathrm{d}x}{x^3} J_1^2(x) + \int_1^\infty \frac{\mathrm{d}x}{x^3} J_1^2(x). \tag{A.21}$$

In the first term we can use $J_1 \approx x/2$ and the second integral is a constant:

$$\begin{aligned} G(u \ll 1, s = 2) &\approx \frac{1}{4} \int_u^1 \frac{\mathrm{d}x}{x} + \text{const.} \\ &= \frac{1}{4} \ln u^{-1} + \text{const.} \end{aligned} \tag{A.22}$$

For the case $s = 2$ we find a logarithmic behaviour of the function $G(u)$. This very particular case in not important for applications.

Appendix B: The integral I_n

Here we discuss the integral

$$I_n(\Lambda, \epsilon, s) = \int_\epsilon^1 \mathrm{d}\mu \frac{\mu^{s+2n+1}}{\left[\epsilon^2 + \Lambda(\mu^2 - \epsilon^2)\right]^{(s+2)/2}} \tag{B.1}$$

for different cases of both parameters Λ and ϵ.

B.1. The case $\Lambda \ll \epsilon^2 \ll 1$

First we apply the transformation

$$x = \frac{\epsilon}{\mu} \sqrt{\frac{1-\Lambda}{\Lambda}} \tag{B.2}$$

to find

$$\begin{aligned} I_n(\Lambda, \epsilon, s) &= \epsilon^{2n} (1-\Lambda)^n \Lambda^{-s/2-n-1} \\ &\quad \times \int_{x_u}^{x_o} \mathrm{d}x \, \frac{x^{-2n-1}}{(1+x^2)^{s/2+1}} \end{aligned} \tag{B.3}$$

with $x_u = \epsilon \sqrt{\frac{1-\Lambda}{\Lambda}}$ and $x_o = \sqrt{\frac{1-\Lambda}{\Lambda}}$. In the case $\Lambda \ll \epsilon^2 \ll 1$, we have

$$x_u \approx \frac{\epsilon}{\sqrt{\Lambda}} \gg 1 \tag{B.4}$$

and

$$x_o \approx \frac{1}{\sqrt{\Lambda}} \gg 1, \tag{B.5}$$

and the integral can be approximated by

$$\begin{aligned} I_n(\Lambda \ll \epsilon^2 \ll 1, s) &\approx \epsilon^{2n} \Lambda^{-s/2-n-1} \int_{x_u}^{x_o} \mathrm{d}x \, x^{-2n-s-3} \\ &= \frac{\epsilon^{-s-2}}{2n+s+2}, \end{aligned} \tag{B.6}$$

which is the final result of this subsection.

B.2. The case $\epsilon^2 \ll \Lambda \ll 1$

In this second case we can also apply Eq. (B.3) but now we have

$$x_u \approx \frac{\epsilon}{\sqrt{\Lambda}} \ll 1 \tag{B.7}$$

and

$$x_o \approx \frac{1}{\sqrt{\Lambda}} \gg 1. \tag{B.8}$$

Therefore we must split the integral

$$\begin{aligned} I_n(\epsilon^2 \ll \Lambda \ll 1, s) &\approx \epsilon^{2n} \Lambda^{-s/2-n-1} \\ &\quad \times \left\{ \int_{x_u}^1 \mathrm{d}x \, x^{-2n-1} + \int_1^{x_o} \mathrm{d}x \, x^{-2n-s-3} \right\}, \end{aligned} \tag{B.9}$$

and we find three cases

$$\begin{aligned} I_{n=0}(\epsilon^2 \ll \Lambda \ll 1, s) &\approx \Lambda^{-s/2-1} \\ &\quad \times \left\{ \frac{1}{s+2} + \ln \epsilon^{-1} + \ln \sqrt{\Lambda} \right\}, \\ I_{n<0}(\epsilon^2 \ll \Lambda \ll 1, s) &\approx \Lambda^{-s/2-1-n} \epsilon^{2n} \\ &\quad \times \left\{ \frac{1}{2n+s+2} - \frac{1}{2n} \right\}, \\ I_{n>0}(\epsilon^2 \ll \Lambda \ll 1, s) &\approx \Lambda^{-s/2-1} \frac{1}{2n}. \end{aligned} \tag{B.10}$$

B.3. The case $\Lambda \approx 1$

Here it is useful to introduce the parameter $\Delta\Lambda := 1 - \Lambda$ to find

$$x_u = \epsilon \sqrt{\frac{\Delta\Lambda}{\Lambda}} \ll 1 \tag{B.11}$$

and

$$x_o = \sqrt{\frac{\Delta\Lambda}{\Lambda}} \ll 1. \tag{B.12}$$

Therefore, the integral can be simplified to

$$\begin{aligned} I_n(\Lambda \approx 1, s) &\approx \epsilon^{2n} (\Delta\Lambda)^n \Lambda^{-s/2-n-1} \\ &\quad \times \int_{x_u}^{x_o} \mathrm{d}x \, x^{-2n-1}. \end{aligned} \tag{B.13}$$

Finally we find three different cases for the nearly isotropic model:

$$\begin{aligned} I_{n=0}(\Lambda \approx 1, s) &\approx \Lambda^{-s/2-1} \ln \epsilon^{-1} \\ I_{n<0}(\Lambda \approx 1, s) &\approx \Lambda^{-s/2-1} \frac{\epsilon^{2n}}{-2n} \\ I_{n>0}(\Lambda \approx 1, s) &\approx \Lambda^{-s/2-1} \frac{1}{2n} \end{aligned} \tag{B.14}$$

B.4. The case $\Lambda \gg 1$

By applying the transformation

$$x = \sqrt{1 - \frac{\epsilon^2}{\mu^2} \frac{\Lambda - 1}{\Lambda}} \tag{B.15}$$

for the integral of Eq. (B.1), we find

$$I_n(\Lambda \gg 1, s) = \epsilon^{2n} \frac{(\Lambda-1)^n}{\Lambda^{s/2+n+1}} \int_{x_u}^{x_o} \mathrm{d}x \, \frac{x^{-s-1}}{(1-x^2)^{n+1}} \tag{B.16}$$

with

$$x_u = \frac{1}{\sqrt{\Lambda}} \ll 1 \tag{B.17}$$

and

$$x_o = \sqrt{1 - \epsilon^2 \frac{\Lambda - 1}{\Lambda}} \approx 1. \tag{B.18}$$

The integral can be expressed by hypergeometric functions

$$\begin{aligned} I_n(\Lambda \gg 1, s) = & \frac{\epsilon^{2n}(\Lambda-1)^n}{s\Lambda^{s/2+n+1}} \\ & \times \Big[x_u^{-s/2}\, {}_2F_1\left(-s/2, n+1, 1-s/2; x_u^2\right) \\ & - x_o^{-s/2}\, {}_2F_1\left(-s/2, n+1, 1-s/2; x_o^2\right)\Big], \end{aligned} \tag{B.19}$$

which can be approximated by

$$\begin{aligned} I_n(\Lambda \gg 1, s) \approx & \frac{\epsilon^{2n}(\Lambda-1)^n}{s\Lambda^{n+1}} \\ & \times {}_2F_1\left(-s/2, n+1, 1-s/2; \frac{1}{\Lambda}\right). \end{aligned} \tag{B.20}$$

Using

$${}_2F_1\left(-s/2, n+1, 1-s/2; \frac{1}{\Lambda}\right) \approx 1 + \frac{s(n+1)}{(s-2)}\Lambda^{-1} \tag{B.21}$$

and

$$(\Lambda - 1)^n \approx \Lambda^n \left(1 - \frac{n}{\Lambda}\right), \tag{B.22}$$

we obtain

$$I_n(\Lambda \gg 1, s) \approx \frac{\epsilon^{2n}}{s\Lambda}\left(1 + \frac{s+2n}{(s-2)\Lambda}\right) \tag{B.23}$$

which is the final result of this subsection.